**Structural Engineering and Mechanics**, *Vol. 62, No. 5 (2017) 519-535*
DOI: https://doi.org/10.12989/sem.2017.62.5.519


# A finite element based assessment of static behavior of multiphase magneto-electro-elastic beams under different thermal loading

M. Vinyas and S.C. Kattimani*

*Department of Mechanical Engineering, National Institute of Technology Karnataka, Surathkal, Mangalore, 575025, India*

*(Received February 13, 2017, Revised March 15, 2017, Accepted March 16, 2017)*

**Abstract.** In this article, static analysis of a magneto-electro-elastic (MEE) beam subjected to various thermal loading and boundary conditions has been investigated. Influence of pyroeffects (pyroelectric and pyromagnetic) on the direct quantities (displacements and the potentials) of the MEE beam under different boundary conditions is studied. The finite element (FE) formulation of the MEE beam is developed using the total potential energy principle and the constitutive equations of the MEE material taking into account the coupling between elastic, electric, magnetic and thermal properties. Using the Maxwell electrostatic and electromagnetic relations, variation of stresses, displacements, electric and magnetic potentials along the length of the MEE beam are investigated. Effect of volume fractions, aspect ratio and boundary conditions on the direct quantities in thermal environment has been determined. The present investigation may be useful in design and analysis of magnetoelectroelastic smart structures and sensor applications.

**Keywords:** magneto-electro-elastic; pyroeffects; direct quantities; temperature profiles; static analysis

## 1. Introduction

In the recent years, smart materials and structures have attracted a considerable interest in the scientific and engineering communities. The drastic developments in the production of advanced composites have paved way for the enhanced utilization of smart structures in numerous applications. It is evident from the extensive research that among the smart materials, piezoelectric (PE) materials are the most widely used materials in smart structures. The self sensing and self diagnosing abilities of these materials enhances the performance of the structures. Hence, many researchers have devoted their study on analyzing the behavior of the PE structures (beams, plates, shells). Temperature is one of the important factor needs to be considered in the analysis of structures because of the fact that the behavior of the structure changes with change in temperature. Hence the analysis of structures made of smart materials in the thermal environment has gained more importance recently. Sharnappa *et al*. (2010) presented a numerical formulation to evaluate the thermally induced vibrations of the piezo-thermo-viscoelastic composite beam. Using the finite element method Rahman *et al*. (2015) presented the dynamic analysis and active vibration control of the piezoelectric beam subjected to thermal loading. The static and dynamic behavior of the thermo piezoelectric smart structures was analysed by Gornandt and Gabbert (2002) using a fully coupled FE iterative solution. Tauchert (1996) developed an exact solution for the piezo thermoelastic problem subjected to steady state temperature distribution. The inherent low-control-authority of piezoelectric materials gave rise to the development of active vibration control of the smart structures. Ray and Batra (2008) proposed a FE formulation for the active vibration control of FG shells subjected to thermal loading using first order shear deformation theory (FSDT). Gupta *et al*. (2011) studied the active vibration control of the smart plate at elevated temperature analytically and compared the results experimentally. Further, the static analysis of these intelligent structures is carried out by many pioneers. Among them, Ray *et al*. (1994) developed a FE model for the static analysis of simply supported rectangular plate using higher order shear deformation (HSDT) theory. Panda and Ray (2008) studied the nonlinear static FE analysis of FG plates in thermal environment. Beni (2016) analysed the piezoelectric nano beam subjected to electrical and mechanical loading considering the size-dependant nonlinear geometry.

The literatures reveal that integration of the ferroelectric and the ferromagnetic properties in a distinct material was cumbersome because of the fact that the atomic phenomenon involved for the ferroelectricity and magnetism do not meddle with each other. Hence, the strong coupling between these two properties was not ensured. With the remarkable progress in the field of material research, an interesting and responsive new smart material known as magneto-electro-elastic (MEE) material was developed. These typical materials are the combination of piezoelectric ($BaTiO_3$) and piezomagnetic ($CoFe_2O_4$) phases. The distinct ability of the MEE materials is to interact with external disturbances and to produce the output signals (electrical / mechanical / magnetic) which makes them suitable for wide range of sensing application such as infrared detection, medical diagnostics, micro-

*Corresponding author, Assistant Professor
E-mail: sck@nitk.ac.in



ISSN: 1225-4568 (Print), 1598-6217 (Online)

electromechanical systems, sonar applications, imaging systems etc. The MEE materials simultaneously possess the coupling between electro-elastic, magneto-elastic and magneto-electric properties. The influence of these coupling effects can be observed in the composite as a whole, but are absent in the individual constituents. It is found that the magneto-electric coupling is many times better than monolithic piezoelectric or piezomagnetic materials. This unique property of the MEE composites makes them capable of converting energy from one form to another (among mechanical, electric and magnetic energies). Multi behavior properties of the MEE composites fetched it a significant importance in a very short span. Research related to magneto-electric effect in elastic media has attracted the focus of the researchers. Pan and Heyliger (2001) presented an exact solution for layered FG-MEE rectangular plate. They found that stacking sequence and boundary conditions have a significant effect on magnetic, electric and elastic fields. Also, they derived an analytical formulation to study the free vibration behavior of the plate. Ramirez *et al*. (2006) presented a solution for free vibration of a 2D MEE laminates using discrete layer approximate model. Kattimani and Ray investigated the active control of geometrically nonlinear vibrations of MEE plates (2014) and doubly curved shells (2014). They also extended their study for the functionally graded MEE plates also (2015). Chen *et al*. (2005) investigated the effect of magneto-electric coupling on the natural frequency of a MEE plate. Chen *et al*. (2007) proposed a general approach to perform the modal analysis of MEE plates using state vector approach and propagator matrix. Bhangale and Ganeshan (2006) derived a semi analytical FE model to study the free vibration analysis of FG-MEE plates. They analysed the effect of exponential factor, mechanical and electrical loading on the induced field. Annigeri *et al*. (2007) studied the free vibrations of multiphase and layerwise MEE beam using FE procedures. Milazzo *et al*. (2009) derived an analytical solution to study the free and forced vibration behavior of MEE bi-morph beam applied with time dependant boundary conditions. Daga *et al*. (2009) investigated the transient response of multiphase MEE cantilever beam using FE method. They have studied the effect of volume fractions and the coupling effect on the response of the beam. Ai-min and Li (2008) proposed an analytical solution which facilitates the analysis of a MEE beam subjected to complex loading and boundary conditions. Xin and Hu (2015) studied the free vibrations of the layered MEE beams using a semi analytical space state approach and discrete singular convolution algorithm which ease the consideration of different boundary conditions. Lage *et al*. (2004) derived a mixed layer wise FE formulation to study the static behavior of the MEE plates. Biju *et al*. (2012 and 2011) investigated the behavior of a MEE sensor patch on a steel beam subjected to harmonic loading. They analysed the transient dynamic behavior of MEE sensors considering the effect of patch location and different boundary conditions on the performance of the beam. In addition, the response of the MEE beam when applied with time harmonic electric potential has also been studied. Vaezi *et al*. (2016) analysed the influence of the electric and magnetic potentials on the natural frequency and buckling loads of the MEE microbeams. Extensive research is also devoted to the prediction of the effective properties of the MEE composites (2013).

The MEE composite in the thermal environment exhibit an additional coupling properties i.e., the thermo-electric (pyroelectric effect) and thermo-magnetic (pyromagnetic effect) properties. They are generally known as the cross or product properties of the materials. These product properties will have a direct or an indirect effect on the stresses, displacements, electric and magnetic potentials of the system through the pyroelectric and pyromagnetic loads. The response of the MEE structures is not only influenced by the material constants, thickness, boundary conditions and the magnitude of the applied fields or loads but also with the variation of the temperature. The study of the response characteristics of the MEE structures under various thermal loading may help to determine the optimum operating conditions of the MEE structures in the thermal environment. Many pioneers have studied the behavior of the MEE structures in thermal environment. With the help of thermodynamic potential Sunar *et al*. (2002) derived the FE model for fully coupled thermopiezomagnetic continuum which has led a way for numerous researches in thermal analysis of the MEE structures. Badri and Kayiem (2013) used the first order shear deformation theory (FSDT) to study the static and dynamic analysis of magneto-thermo-electro-elastic (MTEE) plates. Ebrahimi and Barati (2016) presented an analytical thermal vibration solution of a MTEE nanobeam and demonstrated the effects of thermal loadings, external electric voltage and magnetic potential. Kumaravel *et al*. (2007) investigated the influence of coupling effects on the free vibrations and buckling behavior of the MEE beams in thermal environment. Ansari *et al*. (2015) presented nonlocal nonlinear governing equations of a nano beams subjected to MTEE loads. They analysed the influence of external electric field, magnetic field and temperature changes on the natural frequencies. Jandaghian and Rahmani (2016) studied the free vibration analysis of MTEE beams resting on Pasternak foundation by using nonloacal and Timoshenko beam theory. They found that natural frequency is insensitive to temperature changes. Ootao and Tanigawa (2005) developed an exact solution for the transient behavior of multilayered MTEE strip subjected to non uniform and unsteady heating. Recently, research on the pyroelectric and pyromagnetic effects revealed a mysterious behavior of MEE structures in thermal environment. This interesting phenomenon is studied by many researchers, among them, Kim *et al*. (2012) derived an analytical expression to analyze the product properties of FG transversely isotropic MTEE multilayer composite with an arbitrary number of layers. Kumaravel *et al*. (2007) investigated the behavior of the MEE strip in thermal environment neglecting the pyroelectric and pyromagnetic effects. Challagulla *et al*. (2011) found out the pyroelectric and pyromagnetic constants for various volume fractions of piezoelectric and piezomagnetic materials with the aid of asymptotic homogenization method. Kondaiah *et al*. (2012, 2013a, 2013b) studied the behavior of the MEE beams and plates

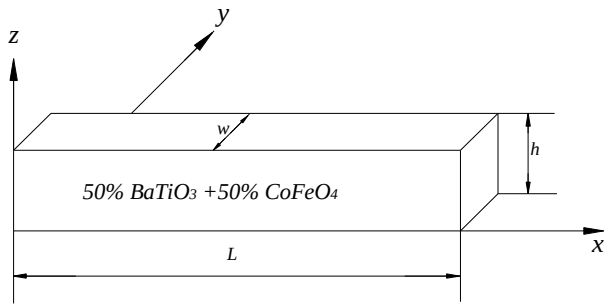


Fig. 1 Magneto-electro-elastic beam

subjected to uniform temperature considering the pyroelectric and pyromagnetic effects. The effect of boundary conditions and volume fractions on the behavior of MEE plates has also been presented. The comprehensive literature review reveals that the research carried out on the MEE structures in thermal environment considering pyroelectric and pyromagnetic effects is limited. However, to the best of the author's knowledge, no work has been reported on the FE analysis of multiphase MEE beam subjected to different thermal loading. Consequently, in the present investigation, the structural behavior of MEE beams under different temperature profiles has been carried out. Influence of temperature profile, product properties, volume fraction, aspect ratio and boundary conditions on the displacement, the electric and magnetic potentials of the MEE beam has been studied comprehensively.

## 2. Basic equations

### *2.1 Problem definition*

The schematic diagram of the MEE beam made up of 50% $BaTiO_3$ and 50% $CoFe_2O_4$ with Cartesian co-ordinate system is shown in Fig. 1. The beam length $L$ is taken along the $x$-direction, while the width $w$ and the thickness $h$ of the MEE beam are taken along the $y$ and $z$-coordinate axes, respectively. The boundary conditions employed for the simply-supported, clamped-clamped and clamped-free MEE beams are as follows:

$u \neq 0, v = w = \phi = \psi = 0$ for the simply supported end

$u = v = w = \phi = \psi = 0$ for the clamped end

$u = v = w = \phi = \psi \neq 0$ for the free end

### *2.2 Constitutive equations*

The constitutive equations for the three dimensional magneto-electro-elastic (MEE) solid considering the linear coupling between thermal, electric, magnetic and mechanical properties in the cartesian co-ordinates can be written as

$$\begin{aligned} \{\sigma\} &= [C]\{\varepsilon\} - \{e\}E - \{q\}H - \{\alpha\}\Delta T \\ D &= \{e\}^T\{\varepsilon\} + \eta E + mH + \{p\}\Delta T \\ B &= \{q\}^T\{\varepsilon\} + mE + \mu H + \{\tau\}\Delta T \end{aligned} \tag{1}$$

where, $[C]$, $\{e\}$, $\{q\}$ and $\{\alpha\}$ are the elastic co-efficient matrix, piezoelectric coefficient matrix, magnetostrictive coefficient matrix and thermal expansion co-efficient matrix, respectively; $\eta$, $m$, $\{p\}$, $\{\tau\}$ and $\mu$ are the dielectric constant, electromagnetic coefficient, pyroelectric constant, pyromagnetic constant and magnetic permeability constant, respectively; $\{\sigma\}$, $D$ and $B$ represent the stress tensor, electric displacement and the magnetic flux, respectively; $\{\mathcal{E}\}$, $E$, $H$ and $\Delta T$ are the linear strain tensor, electric field, magnetic field and temperature rise, respectively. The matrix notation considering all the coefficients appearing in the constitutive relations can be written as

$$\begin{Bmatrix} \sigma_1 \\ \sigma_2 \\ \sigma_3 \\ \tau_{23} \\ \tau_{13} \\ \tau_{12} \\ D_1 \\ D_2 \\ D_3 \\ B_1 \\ B_2 \\ B_3 \end{Bmatrix} = \begin{bmatrix} c_{11} & c_{12} & c_{13} & 0 & 0 & 0 & 0 & 0 \\ c_{12} & c_{11} & c_{13} & 0 & 0 & 0 & 0 & 0 \\ c_{13} & c_{13} & c_{33} & 0 & 0 & 0 & 0 & 0 \\ 0 & 0 & 0 & c_{44} & 0 & 0 & 0 & e_{15} \\ 0 & 0 & 0 & 0 & c_{44} & 0 & e_{15} & 0 \\ 0 & 0 & 0 & 0 & 0 & c_{66} & 0 & 0 \\ 0 & 0 & 0 & 0 & e_{15} & 0 & \eta_{11} & 0 \\ 0 & 0 & 0 & e_{15} & 0 & 0 & 0 & \eta_{11} \\ e_{31} & e_{31} & e_{33} & 0 & 0 & 0 & 0 & 0 \\ 0 & 0 & 0 & 0 & q_{15} & 0 & m_{11} & 0 \\ 0 & 0 & 0 & q_{15} & 0 & 0 & 0 & m_{11} \\ q_{31} & q_{31} & q_{33} & 0 & 0 & 0 & 0 & 0 \end{bmatrix}$$

$$\begin{bmatrix} e_{31} & 0 & 0 & q_{31} \\ e_{31} & 0 & 0 & q_{31} \\ e_{33} & 0 & 0 & q_{33} \\ 0 & 0 & q_{15} & 0 \\ 0 & q_{15} & 0 & 0 \\ 0 & 0 & 0 & 0 \\ 0 & m_{11} & 0 & 0 \\ 0 & 0 & m_{11} & 0 \\ \eta_{33} & 0 & 0 & m_{33} \\ 0 & \mu_{11} & 0 & 0 \\ 0 & 0 & \mu_{11} & 0 \\ m_{33} & 0 & 0 & \mu_{33} \end{bmatrix} \times \left\{ \begin{Bmatrix} \varepsilon_1 \\ \varepsilon_2 \\ \varepsilon_3 \\ \gamma_{23} \\ \gamma_{13} \\ \gamma_{12} \\ E_1 \\ E_2 \\ E_3 \\ H_1 \\ H_2 \\ H_3 \end{Bmatrix} - \begin{Bmatrix} \alpha_1\Delta T \\ \alpha_2\Delta T \\ \alpha_3\Delta T \\ 0 \\ 0 \\ 0 \\ p_1\Delta T \\ p_2\Delta T \\ p_3\Delta T \\ \tau_1\Delta T \\ \tau_2\Delta T \\ \tau_3\Delta T \end{Bmatrix} \right\} \tag{2}$$

### *2.3 Finite Element (FE) formulation*

The MEE beam is discretized into 10 finite elements (FE) using an eight noded 3D brick element. Each element is assumed to have five degrees of freedom *viz.* three translational [$u$ $v$ $w$], one electric and magnetic potential. The generalized translational displacement vector associated with the $i^{th}$ ($i$ = 1, 2, 3,…, 8) node of the element can be represented as

$$\{d_{ti}\} = [u_i \;\; v_i \;\; w_i]^T \tag{3}$$

The generalized displacement vector $\{d_t\}$, electric potential vector $\{\phi\}$ and magnetic potential vector $\{\psi\}$ at any point within the element can be represented in terms of the nodal generalized displacement vector, the nodal electric potential vector and the nodal magnetic potential

vector, respectively as follows

$$\{d_t\}=[N_t]\{d_t^e\},\ \{\phi\}=[N_\phi]\{\phi^e\},\ \{\psi\}=[N_\psi]\{\psi^e\} \quad (4)$$

The various elemental vectors appearing in Eq. (4) can be represented as

$$\{d_t^e\}=\left[\{d_{t1}\}^T\{d_{t2}\}^T\ldots\ \{d_{t8}\}^T\right]^T,\ \{\phi^e\}=[\phi_1\ \phi_2\ \ldots\ \phi_8]^T,$$
$$\{\psi^e\}=[\psi_1\ \psi_2\ \ldots\ \psi_8]^T,\ [N_t]=[N_{t1}\,N_{t2}\ \ldots\ N_{t8}],$$
$$N_{ti}=n_i I_t,\ [N_\phi]=[n_1\ n_2\ldots\ n_8],\ [N_\psi]=[n_1\,n_2\ldots n_8] \quad (5)$$

where, $n_i$ is the natural coordinate shape function associated with the i[th] node of the element; *'$I_t$'* is the identity matrix; $[N_t]$, $[N_\phi]$ and $[N_\psi]$ are $(3\times24)$, $(1\times8)$ and $(1\times8)$ shape function matrices, respectively. In the absence of free charge density, the Gauss law can be written as $\nabla D=0$. Then the relation between the electric field $E$ and the electric potential $\phi$ can be expressed as $E=-\nabla\phi$. Similarly, in the absence of free current density, the magnetic field can be expressed as $\nabla B=0$, for which the relation between the magnetic field $H$ and the magnetic potential $\psi$ can be written as $H=-\nabla\psi$. The gradient relation corresponding to the linear electric field ($E$) and the electric potential ($\phi$) can be written using the Maxwell's equation as follows

$$\{E\}=\left\{-\frac{\partial\phi}{\partial x},-\frac{\partial\phi}{\partial y},-\frac{\partial\phi}{\partial z}\right\} \quad (6)$$

While the relation between the magnetic field ($H$) and the magnetic potential ($\psi$) can also be expressed as

$$\{H\}=\left\{-\frac{\partial\psi}{\partial x},-\frac{\partial\psi}{\partial y},-\frac{\partial\psi}{\partial z}\right\} \quad (7)$$

The strain vector, electric potential vector and magnetic potential vector of the system can be related to the nodal displacement, nodal electric potential and nodal magnetic potential, respectively, with the aid of the derivative of shape function matrices as follows

$$\{\varepsilon\}=[B_t]\{d_t^e\},\{H\}=[B_\psi]\{\psi^e\},\{E\}=[B_\phi]\{\phi^e\} \quad (8)$$

The shape function derivative matrices appearing in Eq. (8) are represented by

$$[B_t]=[B_{t1}\,B_{t2}\ldots\,B_{t8}],\ [B_\psi]=[B_{\psi1}\,B_{\psi2}\ldots\,B_{\psi8}]$$
$$[B_\phi]=[B_{\phi1}\,B_{\phi2}\ldots\,B_{\phi8}] \quad (9)$$

in which, the sub matrices, $[B_{ti}]$, $[B_{\psi i}]$ and $[B_{\phi i}]$ are given by

$$[B_{ti}]=\begin{bmatrix}\frac{\partial n_i}{\partial x}&0&0\\0&\frac{\partial n_i}{\partial y}&0\\0&0&\frac{\partial n_i}{\partial z}\\0&\frac{\partial n_i}{\partial z}&\frac{\partial n_i}{\partial y}\\\frac{\partial n_i}{\partial z}&0&\frac{\partial n_i}{\partial x}\\\frac{\partial n_i}{\partial y}&\frac{\partial n_i}{\partial x}&0\end{bmatrix},[B_{\psi i}]=\begin{bmatrix}\frac{-\partial n_i}{\partial x}\\-\frac{\partial n_i}{\partial y}\\-\frac{\partial n_i}{\partial z}\end{bmatrix},[B_{\phi i}]=\begin{bmatrix}\frac{-\partial n_i}{\partial x}\\-\frac{\partial n_i}{\partial y}\\-\frac{\partial n_i}{\partial z}\end{bmatrix} \quad (10)$$

where, $i$=1, 2, 3,..., 8 represents the node number

### 2.4 Equations of motion

The governing equations of the MEE beam in thermal environment can be derived by employing the principle of total potential energy as follows

$$T_p=\frac{1}{2}\int_\Omega\{\varepsilon\}^T\{\sigma\}d\Omega-\frac{1}{2}\int_\Omega\{E\}^T\{D\}d\Omega-\frac{1}{2}\int_\Omega\{H\}^T\{B\}d\Omega$$
$$-\int_A\{d_t\}^T\{f\}dA-\int_A\phi\,Q^\phi dA-\int_A\psi\,Q^\psi dA \quad (11)$$

where, $\{f\}$ is the surface force vector acting over an area $A$. The entire volume of the domain is represented by $\Omega$. The surface electric charge density and surface magnetic charge density are represented by $Q^\phi$ and $Q^\psi$, respectively. Substituting Eq. (1) into Eq. (11), we get

$$\begin{aligned}T_p=&\frac{1}{2}\int_\Omega\{\varepsilon\}^T[C]\{\varepsilon\}d\Omega-\frac{1}{2}\int_\Omega\{\varepsilon\}^T[e]\{E\}d\Omega\\&-\frac{1}{2}\int_\Omega\{\varepsilon\}^T[q]\{H\}d\Omega-\frac{1}{2}\int_\Omega\{\varepsilon\}^T[C]\{\alpha\}\Delta Td\Omega\\&-\frac{1}{2}\int_\Omega\{E\}^T[e]^T\{\varepsilon\}d\Omega-\frac{1}{2}\int\{E\}^T[\eta]\{E\}d\Omega\\&-\frac{1}{2}\int_\Omega\{E\}^T[m]\{H\}d\Omega-\frac{1}{2}\int_\Omega\{E\}^T\{p\}\Delta Td\Omega\\&-\frac{1}{2}\int\{H\}^T[q]^T\{\varepsilon\}d\Omega--\frac{1}{2}\int\{H\}^T[m]\{E\}d\Omega\\&-\frac{1}{2}\int\{H\}^T[\mu]\{H\}d\Omega-\frac{1}{2}\int\{H\}^T\{\tau\}\Delta Td\Omega\\&-\int_A\{d_t\}^T\{f\}dA-\int_A\{\phi\}Q^\phi dA-\int_A\{\psi\}Q^\psi dA\end{aligned} \quad (12)$$

Now, on substituting Eq. (8) in Eq. (12), we obtain

$$\begin{aligned}T_p^e=&\frac{1}{2}\int_\Omega\{d_t^e\}^T[B_t]^T[C][B_t]\{d_t^e\}d\Omega-\frac{1}{2}\int_\Omega\{d_t^e\}^T[B_t]^T[e][B_\phi]\{\phi^e\}d\Omega\\&-\frac{1}{2}\int_\Omega\{d_t^e\}^T[B_t]^T[q][B_\psi]\{\psi^e\}d\Omega-\frac{1}{2}\int_\Omega\{d_t^e\}^T[B_t]^T[C]\{\alpha\}\Delta Td\Omega\\&-\frac{1}{2}\int_\Omega\{\phi^e\}^T[B_\phi]^T[e]^T[B_t]\{d_t^e\}d\Omega-\frac{1}{2}\int_\Omega\{\phi^e\}^T[B_\phi]^T[\eta][B_\phi]\{\phi^e\}d\Omega\\&-\frac{1}{2}\int_\Omega\{\phi^e\}^T[B_\phi]^T[m][B_\psi]\{\psi^e\}d\Omega-\frac{1}{2}\int_\Omega\{\phi^e\}^T[B_\phi]^T\{p\}\Delta Td\Omega\\&-\frac{1}{2}\int_\Omega\{\psi^e\}^T[B_\psi]^T[q]^T[B_t]\{d_t^e\}d\Omega-\frac{1}{2}\int_\Omega\{\psi^e\}^T[B_\psi]^T[m][B_\phi]\{\phi^e\}d\Omega\\&-\frac{1}{2}\int_\Omega\{\psi^e\}^T[B_\psi]^T[\mu][B_\psi]\{\psi^e\}d\Omega-\frac{1}{2}\int_\Omega\{\psi^e\}^T[B_\psi]^T[\tau]\Delta Td\Omega\\&-\int_A\{d_t^e\}^T[N_t]^T\{f^e\}dA\\&-\int_A\{\phi^e\}[N_\phi]Q^\phi dA\\&-\int_A\{\psi^e\}[N_\psi]Q^\psi dA\end{aligned} \quad (13)$$

The total potential energy is minimized by setting its first variation of Eq. (11) to zero.

$$T_p=\frac{1}{2}\int_\Omega\delta\{\varepsilon\}^T\{\sigma\}d\Omega-\frac{1}{2}\int_\Omega\delta\{E\}^T\{D\}d\Omega$$

$$-\frac{1}{2}\int_{\Omega}\delta\{H\}^{T}\{B\}d\Omega-\int_{A}\delta\{d_t\}^{T}\{f\}dA$$
$$-\int_{A}\delta\{\phi\}Q^{\phi}dA-\int_{A}\delta\{\psi\}Q^{\psi}dA=0 \quad (14)$$

Further, it is assumed that the temperature field is not fully coupled with MEE field. On simplification of the Eqs. (12)-(14), we obtain the equations of motions for the MEE Beam subjected to a temperature deviation of $\Delta T$ as follows

$$\begin{bmatrix}K_{tt}^{e}\end{bmatrix}\{d_t^{e}\}+\begin{bmatrix}K_{t\phi}^{e}\end{bmatrix}\{\phi^{e}\}+\begin{bmatrix}K_{t\psi}^{e}\end{bmatrix}\{\psi^{e}\}=\{F_m^{e}\}+\{F_{th}^{e}\}$$
$$\begin{bmatrix}K_{t\phi}^{e}\end{bmatrix}^{T}\{d_t^{e}\}-\begin{bmatrix}K_{\phi\phi}^{e}\end{bmatrix}\{\phi^{e}\}-\begin{bmatrix}K_{\phi\psi}^{e}\end{bmatrix}\{\psi^{e}\}=\{F_{\phi}^{e}\}-\{F_{p.e}^{e}\}$$
$$\begin{bmatrix}K_{t\psi}^{e}\end{bmatrix}^{T}\{d_t^{e}\}-\begin{bmatrix}K_{\phi\psi}^{e}\end{bmatrix}^{T}\{\phi^{e}\}-\begin{bmatrix}K_{\psi\psi}^{e}\end{bmatrix}\{\psi^{e}\}=\{F_{\psi}^{e}\}-\{F_{p.m}^{e}\} \quad (15)$$

The various elemental stiffness matrices appearing in Eq. (15) are the elemental elastic stiffness matrix $[K_{tt}^{e}]$, the elemental electro-elastic coupling stiffness matrix $[K_{t\phi}^{e}]$, the elemental magneto-elastic coupling stiffness matrix $[K_{t\psi}^{e}]$, the elemental electric stiffness matrix $[K_{\phi\phi}^{e}]$, the elemental magnetic stiffness matrix $[K_{\psi\psi}^{e}]$, the elemental electro-magnetic stiffness matrix $[K_{\phi\psi}^{e}]$. The explicit forms of these matrices are given as follows

$$\begin{bmatrix}K_{tt}^{e}\end{bmatrix}=\int_{\Omega}\begin{bmatrix}B_t\end{bmatrix}^{T}[C]\begin{bmatrix}B_t\end{bmatrix}d\Omega,\ \begin{bmatrix}K_{t\phi}^{e}\end{bmatrix}=\int_{\Omega}\begin{bmatrix}B_t\end{bmatrix}^{T}[e]\begin{bmatrix}B_{\phi}\end{bmatrix}d\Omega,$$
$$\begin{bmatrix}K_{t\psi}^{e}\end{bmatrix}=\int_{\Omega}\begin{bmatrix}B_t\end{bmatrix}^{T}[q]\begin{bmatrix}B_{\psi}\end{bmatrix}d\Omega,\ \begin{bmatrix}K_{\phi\phi}^{e}\end{bmatrix}=\int_{\Omega}\begin{bmatrix}B_{\phi}\end{bmatrix}^{T}[\eta]\begin{bmatrix}B_{\phi}\end{bmatrix}d\Omega,$$
$$\begin{bmatrix}K_{\phi\psi}^{e}\end{bmatrix}=\int_{\Omega}\begin{bmatrix}B_{\phi}\end{bmatrix}^{T}[m]\begin{bmatrix}B_{\psi}\end{bmatrix}d\Omega,$$
$$\begin{bmatrix}K_{\psi\psi}^{e}\end{bmatrix}=\int_{\Omega}\begin{bmatrix}B_{\psi}\end{bmatrix}^{T}[\mu]\begin{bmatrix}B_{\psi}\end{bmatrix}d\Omega \quad (16)$$

Similarly, the various elemental load vectors described in Eq. (15) are the elemental mechanical load vector $\{F_m^{e}\}$, the elemental thermal load vector $\{F_{th}^{e}\}$, the elemental electric charge load vector $\{F_{\phi}^{e}\}$, the elemental magnetic current load vector $\{F_{\psi}^{e}\}$, the elemental pyroelectric load vector $\{F_{p.e}^{e}\}$, the elemental pyromagnetic load vector $\{F_{p.m}^{e}\}$. These load vectors are given by

$$\{F_m^{e}\}=\int_{A}\begin{bmatrix}N_t\end{bmatrix}^{T}f\ dA,\ \{F_{\phi}^{e}\}=\int_{A}\begin{bmatrix}N_{\phi}\end{bmatrix}^{T}Q^{\phi}dA,$$
$$\{F_{\psi}^{e}\}=\int_{A}\begin{bmatrix}N_{\psi}\end{bmatrix}^{T}Q^{\Psi}dA,\ \{F_{th}^{e}\}=\int_{\Omega}\begin{bmatrix}B_t\end{bmatrix}^{T}[C]\{\alpha\}\Delta Td\Omega$$
$$\{F_{p.e}{}^{e}\}=\int_{\Omega}\begin{bmatrix}B_{\phi}\end{bmatrix}^{T}[p]\Delta Td\Omega,$$
$$\{F_{p.m}{}^{e}\}=\int_{\Omega}\begin{bmatrix}B_{\psi}\end{bmatrix}^{T}[\tau]\Delta Td\Omega \quad (17)$$

Considering only the thermal, the pyroelectric and the pyromagnetic loads, the elemental equations of motion are assembled in the straight forward manner into global equations of motion of the MEE beams as follows

$$\begin{bmatrix}K_{tt}\end{bmatrix}\{d_t\}+\begin{bmatrix}K_{t\phi}\end{bmatrix}\{\phi\}+\begin{bmatrix}K_{t\psi}\end{bmatrix}\{\psi\}=\{F_{th}\}$$
$$\begin{bmatrix}K_{t\phi}\end{bmatrix}^{T}\{d_t\}-\begin{bmatrix}K_{\phi\phi}\end{bmatrix}\{\phi\}-\begin{bmatrix}K_{\phi\psi}\end{bmatrix}\{\psi\}=\{F_{p.e}\}$$
$$\begin{bmatrix}K_{t\psi}\end{bmatrix}^{T}\{d_t\}-\begin{bmatrix}K_{\phi\psi}\end{bmatrix}^{T}\{\phi\}-\begin{bmatrix}K_{\psi\psi}\end{bmatrix}\{\psi\}=\{F_{p.m}\} \quad (18)$$

where, $[K_{tt}]$, $[K_{t\phi}]$, $[K_{t\psi}]$, $[K_{\phi\psi}]$, $[K_{\phi\phi}]$ and $[K_{\psi\psi}]$ are the global elastic stiffness matrix, global electro-elastic coupling stiffness matrix, global magneto-elastic coupling stiffness matrix, global electro-magnetic stiffness matrix, global electric stiffness matrix and the global magnetic stiffness matrix, respectively. $\{F_{th}\}$, $\{F_{p.e}\}$ and $\{F_{p.m}\}$ are the global thermal load vector, global pyroelectric load vector and global pyromagnetic load vector, respectively. By eliminating the electric and magnetic potentials in Eq. (18) through the condensation method we obtain

$$[K_{eq}]\{u\}=\{F_{eq}\} \quad (19)$$

The nodal thermal displacements are obtained by solving the Eq. (19). The various stiffness matrices and load vectors involved in attaining Eq. (19) are presented in Appendix. The Gaussian integration with four points is invoked to evaluate the integrals of various elemental stiffness matrices and load vectors. Once the nodal displacements are obtained, the electric and the magnetic potentials are evaluated.

## 3. Temperature fields

In the real time application, the beam or structures generally experiences four different types of temperature variations which are considered here for the analysis. The one-dimensional temperature fields are assumed to vary along the length $L$ of the beam. In all cases the maximum temperature ($T_{max}$) is considered to be 100 K.

### *3.1 Uniform temperature profile (Temperature Profile-1)*

The temperature of the MEE beam is uniformly raised from a reference temperature of $T_0$ to the final temperature of $T_{max}$. For the ease of calculation $T_0$ is assumed to be 0 K. The general temperature variation relation can be written as

$$\Delta T_1 = T_{max} - T_0 \quad (20)$$

### *3.2 Half-Sine temperature profile (Temperature Profile-2)*

The MEE beam is analysed for the half - sine temperature loading. The temperature of the beam is assumed to vary along the length of the beam resembling a half sine wave with a peak at the midspan of the beam. The general equation corresponding to the half-sine wave can be written as

$$\Delta T_2 = T_{max}\{\sin(\frac{\pi x}{L})\} \qquad 0 \le x \le L \quad (21)$$

in which, $T_{max}$ is the maximum temperature, $L$ is the span length of the beam, $x$ is the point of interest from the left support of the beam.

### *3.3 Linearly varying temperature profile. (Temperature Profile-3)*

In this case, the static analysis of the MEE beam is carried out for linearly varying temperature load varying from a certain initial temperature at the left end of the beam $T_i$ to the maximum temperature $T_{\max}$. The corresponding general equation may be expressed as

$$\Delta T_3 = \{T_{max}\}\, x + \{T_i\} \qquad 0 \le x \le L \tag{22}$$

### *3.4 Tent shaped or Bi-triangular temperature profile (Temperature Profile-4)*

In this case, the MEE beam is exposed to a bi-triangular distribution temperature profile i.e,, the temperature of the beam decreases from the $T_{\max}$ at the left support to the lowest possible temperature at the mid span of the beam and again rises to the $T_{\max}$ at the right end of the beam. The above characteristic temperature variation can be represented by the equation as follows

$$\begin{aligned} \Delta T_4 &= \{T_{max}\} \times (1 - x) \quad 0 \le x \le L/2 \\ \Delta T_4 &= \{T_{max}\} \times (x) \qquad a/2 \le x \le L \end{aligned} \tag{23}$$

## 4. Results and discussion

In this section, the numerical results are evaluated using the finite element (FE) model derived in the previous section. The static behavior of the magneto-electro-elastic (MEE) beam is analysed for different boundary conditions and temperature profiles. The boundary conditions considered for the analysis are clamped-clamped (C-C), clamped-free (C-F) and clamped-simply supported (C-S). The MEE beam is assumed to be transversely isotropic in both piezoelectric and piezomagnetic phases (symmetric about *z*-axis). The material properties for different volume fraction of the MEE material are tabulated in Kondaiah *et al*. (2012). The volume fraction ($V_f$) of the MEE beam is taken as 0.5 (50% $BaTiO_3$ and 50% $CoFe_2O_4$) unless otherwise stated. The dimensions of the beam considered for the analysis are length $L$=1 m, width $w$=0.1 m and thickness $h$=0.1 m. The influence of volume fraction and pyroeffects (coupling effects of thermo-electric and thermo-magnetic properties) on the direct quantities (displacements and potentials) are studied for C-C and C-S boundary conditions and compared with the conventional approach (neglecting pyroeffects). Further, the effect of the ratio of the span length to the thickness of the beam ($L/h$) on the potentials of the MEE beam has been investigated.

### *4.1 Validation of the present formulation*

The present FE formulation is validated with the results reported by Kondaiah *et al*. (2012) for the identical boundary conditions, geometry of the beam, loading conditions and material properties. Figs. 2(a)-(e) illustrate the validation of the displacements along longitudinal *x*-direction ($U_x$), electric potential, magnetic potential and normal stresses. It may be observed from these figures that

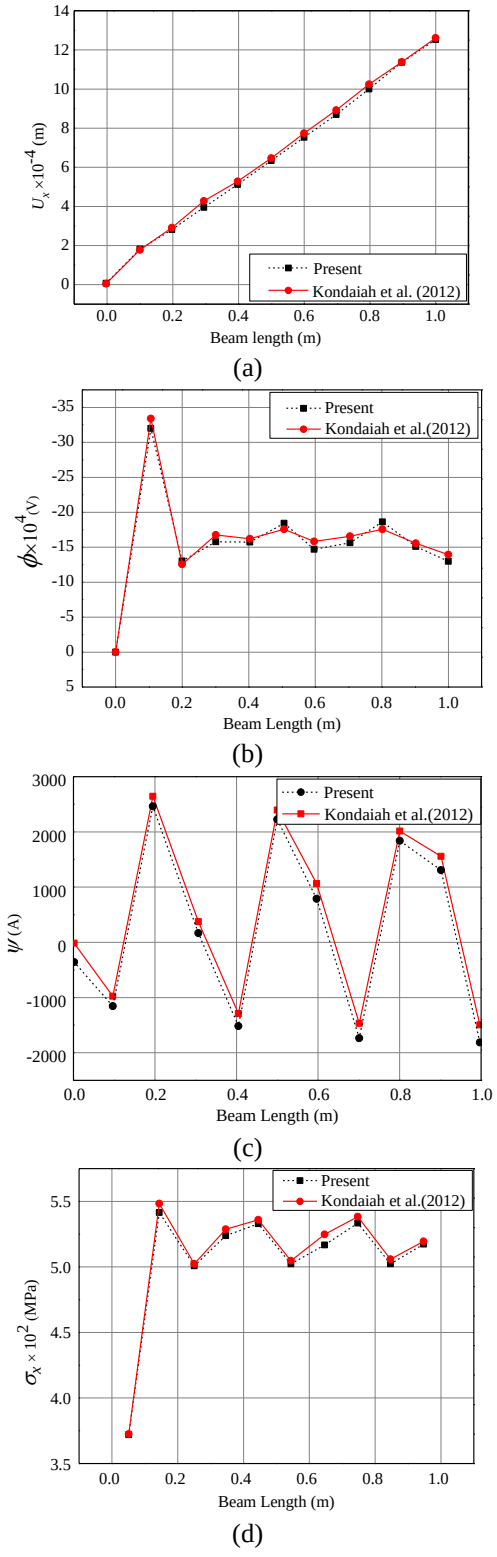


Fig. 2 Validation of (a) longitudinal *x*-direction ($U_x$) (b) electric potential ($\phi$) (c) magnetic potential ($\psi$) (d) normal stress-$\sigma_x$

the results are in excellent agreement with the results reported by Kondaiah *et al*. (2012). It is evident from these figures that the present FE formulation can faithfully produce the results for different boundary conditions and temperature profiles.

### *4.2 Static analysis of MEE beam*

#### *4.2.1 Clamped-Free (C-F) boundary condition*

Influence of various temperature profiles on the structural behavior of the clamped-free (C-F) MEE beam has been investigated. The geometrical parameters and the material properties of the MEE beam remain invariant. The different temperature profiles mentioned in the Eqs. (20)-(23) have been considered for the static analysis. It has been observed from the results reported in the literature by Kondaiah *et al*. (2012) that for the clamped free MEE beam subjected to uniform temperature rise of 100 K, the pyroeffects are dominant only in the variation of the electric potential. The same is verified in the present analysis and extended the analysis for different temperature profiles. It is observed from the numerical simulations that irrespective of the temperature profile, the influence of the thermo-electric (pyroelectric) and the thermo-magnetic (pyromagnetic) coupling effects exist only for the electric potential of the C-F MEE beam. Hence, for the sake of brevity, the comparison between the pyroeffects and the conventional approach is presented only for the electric potential as elucidated in Figs. 3(a)-(d). It may be observed from these figures that for all the temperature profiles the pyroeffects tends to improve the electric potential of the C-F MEE beam. Figs. 4(a)-(c) illustrate the influence of the temperature profiles on the displacement components along *x*, *y* and *z*-directions, respectively, at the nodes along the bottom edge of the MEE beam. It may be noticed from these figures that the longitudinal *x*-direction displacement component $U_x$ varies almost linearly for all the temperature profiles and it is maximum at the free end of the MEE beam. Among all the temperature profiles, the maximum displacement of $U_x$, $U_y$ and $U_w$ is observed for the uniform temperature profile (temperature profile-1). The displacement components $U_y$ and $U_w$ are maximum at the region near the clamped end for the uniform (temperature profile-1) and bi-triangular temperature profiles (temperature profile-4) while for the half-sine (temperature profile-2) and linear temperature profiles (temperature profile-3), the maximum values of these displacement components are witnessed at the midspan and free end of the MEE beam, respectively. This may be due to the maximum temperature value at the respective regions. Fig. 4(d) depict the magnetic potential variation along the MEE beam length for different temperature profiles. It may also be observed that the magnetic potential is maximum for the temperature profile-1 and 4 while the temperature profile 2 and 3 exhibit negligible influence on the variation of magnetic potential.

Figs. 5 (a)-(c) demonstrate the variation of normal stresses for clamped-free (C-F) MEE beam subjected to different temperature profiles. It may be observed from these figures that for the temperature profile-1 and 4, the maximum normal stresses are observed near the clamped end of the beam. This may be due to the presence of constraints and highest temperature in the corresponding profile. For the temperature profile-2, the normal stresses vary symmetrically along the beam length while a linear variation in the normal stresses is observed for temperature profile-3. At the mid-span of the beam, the maximum and

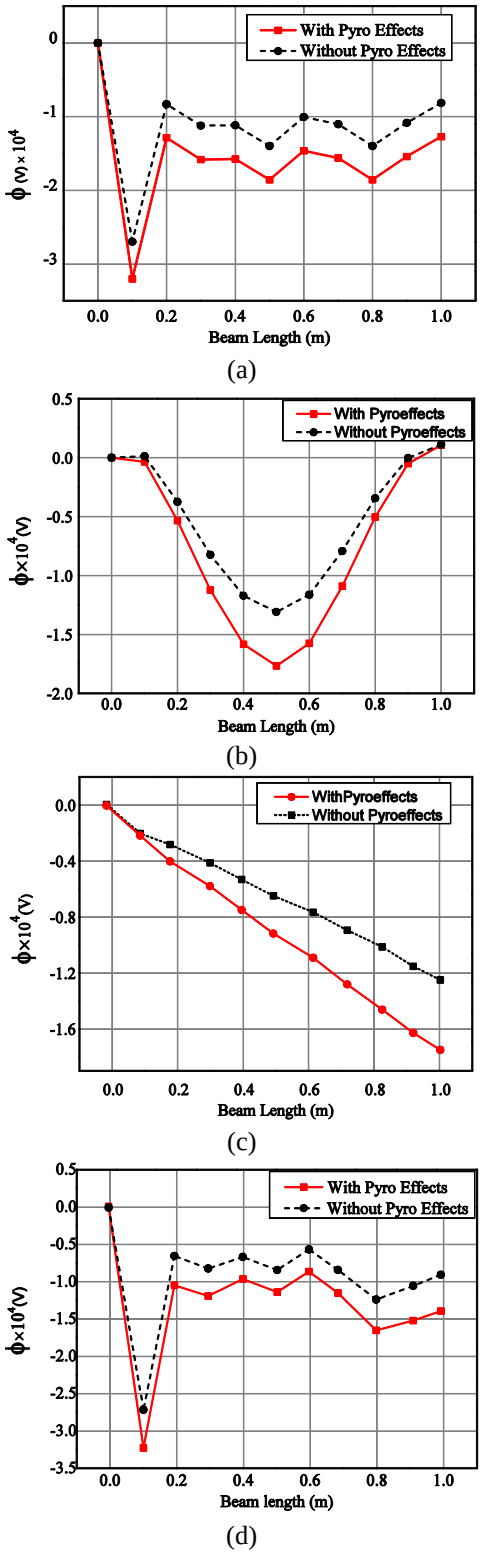


Fig. 3 Variation of electric potential ($\phi$)-(a) uniform temerature (b) half-sine temperature (c) linear temperature profile (d) bi-triangular temperature profile for C-F boundary condition

the minimum normal stresses are noticed for temperature profile-2 and 4, respectively. This may be due to the fact that the temperature at the midspan is maximum for the temperature profile-2 and minimum for the temperature

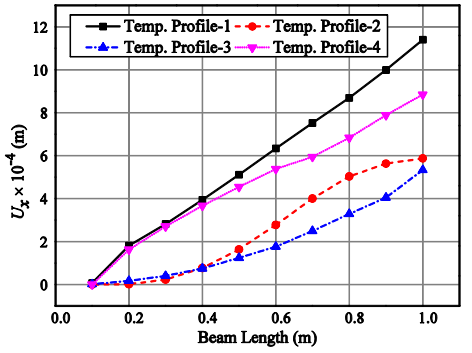


(a)

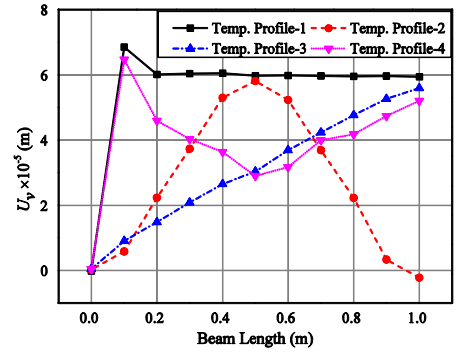


(b)

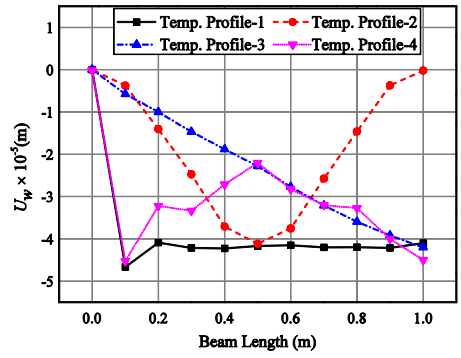


(c)

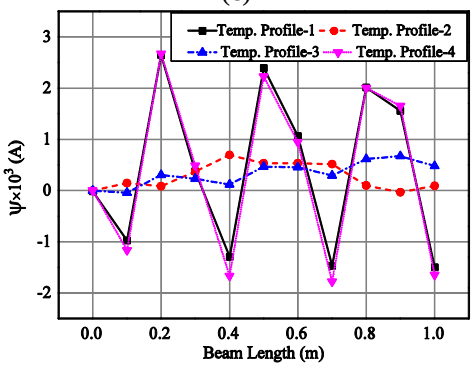


(d)

Fig. 4 Effect of temperature profiles on (a) longitudinal $x$-direction displacement component ($U_x$) (b) $y$-direction displacement component ($U_y$) (c) $z$-direction displacement component (d) magnetic potential ($\psi$) -C-F boundary condition

profile-4. It may be seen from these figures that the temperature profile-1 has a predominant effect on the normal stresses. The variations of the transverse shear

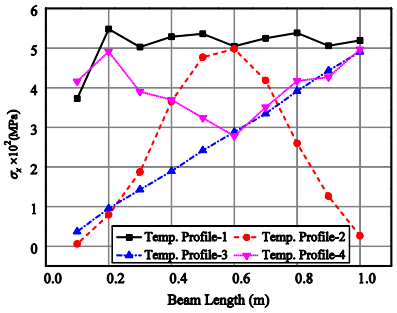


(a)

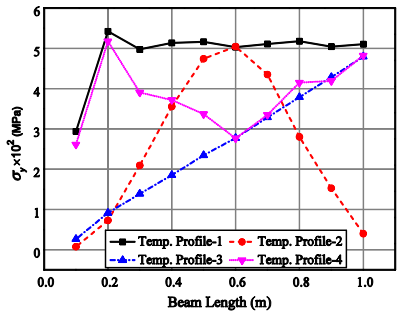


(b)

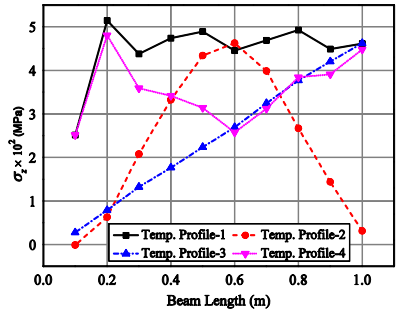


(c)

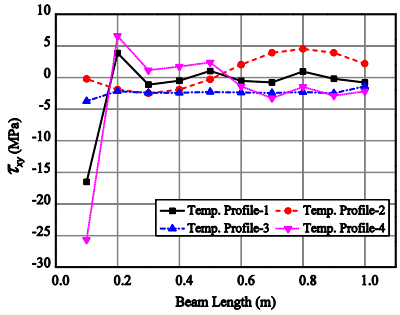


(d)

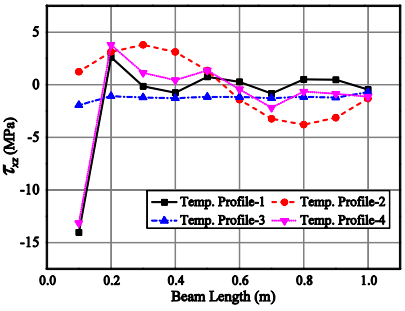


(e)

Fig. 5 Effect of temperature profiles (a) normal stress ($\sigma_x$) (b) normal stress ($\sigma_y$) (c) normal stress ($\sigma_z$) (d) shear stress ($\tau_{xy}$) (e) shear stress ($\tau_{xz}$) along the length of the C-F MEE beam

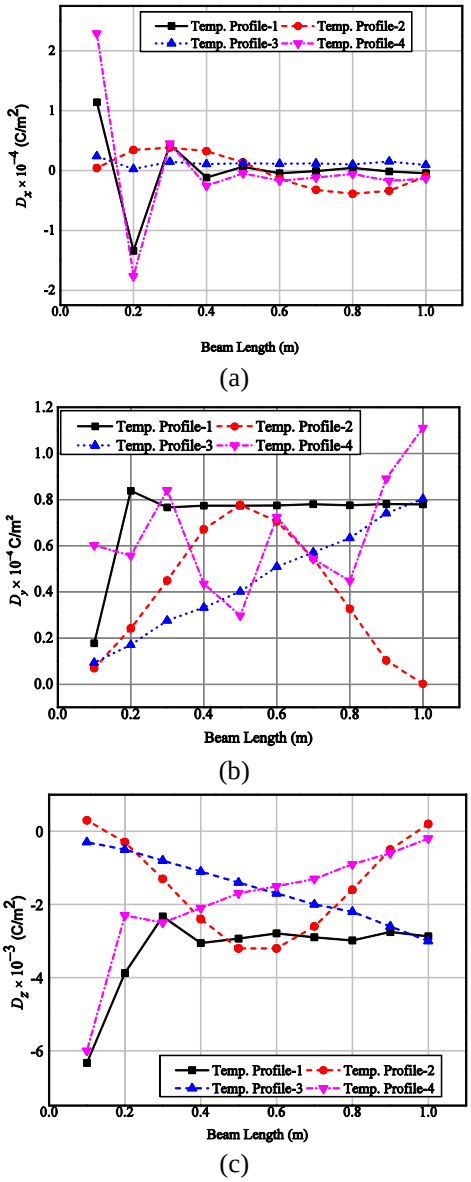


Fig. 6 Effect of temperature profiles on electric displacement (a) $D_x$ (b) $D_y$ (c) $D_z$

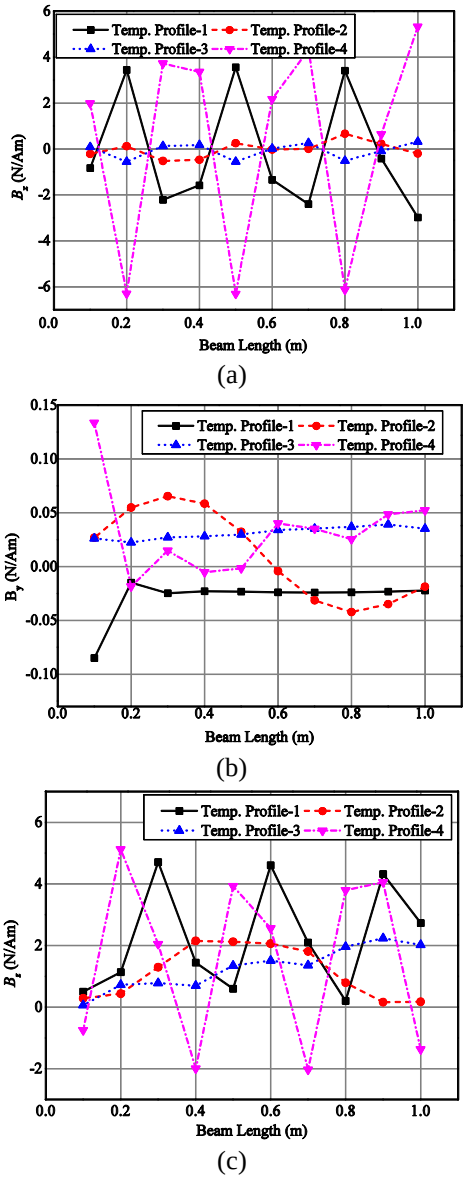


Fig. 7 Effect of temperature profiles on magnetic induction (a) $B_x$ (b) $B_y$ (c) $B_z$

stresses $\tau_{xy}$ and $\tau_{xz}$ are plotted in Figs. 5(d) and (e), respectively. It may be observed that for the temperature profile-2, the shear stresses $\tau_{xy}$ and $\tau_{xz}$ are zero at the mid span with a symmetrical variation along the beam length. However, for the temperature profile-3, the shear stresses along the beam length are constant. It may be observed from these figures that among all the temperature profiles considered, the shear stresses are maximum near the clamped end for temperature profile-4. The present numerical simulation reveals that irrespective of the teperature profiles, the pyroelectric and pyromagnetic loads have negligable effect on the displacements and stresses in comparison with the conventional approach. Therefore, these results are not included here for the sake of brevity. This may be because of the fact that the displacements are governed directly by the thermal loading in the system and indirectly by the pyroeffect. Pyroeffects exhibits a direct influence only on the potentials of the system. From the Figs. 3 and 4(d), it is evident that the effect of thermo-electric and thermo-magnetic coupling (pyroeffects) are dominant on the electric potential but have negligible effect on the magnetic potential. This may be due to negligable pyromagnetic effect on the uncoupled magnetic potential against the significant pyroelectric effect on the uncoupled electric potential (Kondaiah *et al*. 2012).

The effect of the temperature profiles on the variation of the electric displacement components in *x*, *y* and *z*-direction are illustrated in Figs. 6(a)-(c), respectively. It may be observed from Fig. 6(a) that a similar trend of variation in *x*-direction electric displacement components $D_x$ is followed by the temperature profiles 1 and 4. Also, $D_x$ for temperature profile-2 varies symmetrically along the beam length. From Fig. 6(b), it is witnessed that *y*-direction electric displacement components $D_y$ for the temperature profile-2 and 3 follows the corresponding temperature distribution. Further, *z*-direction electric displacement

components $D_z$ for temperature profile 2 and 3 varies similar to that of $D_y$ as depicted in Fig. 6(c). The magnetic flux density variation of the MEE beam with various temperature profile is shown in Figs. 7(a)-(c). It may be observed that the significant influence of the bi-triangular temperature profile (temperature profile-4) on the magnetic flux density components $B_x$, $B_y$ and $B_z$ is noticed.

#### *4.2.2 Clamped-Clamped (C-C) Boundary condition*

The clamped-clamped (C-C) MEE beam subjected to different temperature loading profiles is considered for the analysis. It is known that the direct quantities (displacements and potentials) affect the derived quantities (stresses, electrical displacements and magnetic density) of the MEE beam. Hence, it is important to study the effect of the direct quantities on the behavior of the MEE beam. The effect of different temperature profiles on the direct quantities of the C-C MEE beam is presented in Figs. 8(a)-(e). It may be noticed from Fig. 8(a) that when the beam is subjected to temperature profile-1 (uniform temperature), the displacement component $U_x$ is minimum and this varies accordingly with the temperature profile. At the midspan of the beam, $U_x$ is maximum for the temperature profile-3 while it is zero for the remaining temperature profiles. Fig. 8(b) depicts the variation of $U_v$ along the beam length. It may be observed from this figure that $U_v$ reaches a higher value for the uniform temperature profile compared to the remaining temperature profiles. For the temperature profile-3, $U_v$ varies linearly along the beam length while the maximum displacement is noticed near the right end of the beam. For the temperature profile-2, $U_v$ is maximum at the midspan whereas, it is minimum for temperature profile-4. These displacements variations are expected as an outcome of the respective temperature distribution. Also, it is evident from Fig. 8(c) that $U_w$ follows the same characteristics of $U_v$. It may also be observed from Fig. 8(d) that for all the temperature profiles, the maximum value of electric potential is noticed at the region near the clamped end while at the mid-span of the beam, the minimum electric potential is noticed for the temperature profile-2 compared to other temperature profiles. Also, along the beam length electric potential varies linearly for temperature profile-3 while for the temperature profile-4, the electric potential follows the same trend as that of the temperature profile-1. Fig. 8(e) demonstrates the effect of temperature loading on the magnetic potential. The maximum magnetic potential is observed when the MEE beam is subjected to uniform temperature (temperature profile-1). For the half-sine temperature profile (temperature profile-2), the maximum magnetic potential may be observed at the mid span of the beam. It may be noticed from this figure that among all the temperature loadings the temperature profile-1 has a significant effects on direct quantities. This may be due to the constant pyro loads (pyroelectric and pyromagnetic) generated along the length of the MEE beam.

#### *4.2.3 Clamped-Simply supported (C-S) boundary condition*

The variation of the direct quantities in a clamped-simply supported (C-S) MEE beam for different temperature profiles are depicted in Figs. 9(a)-(e). It may be

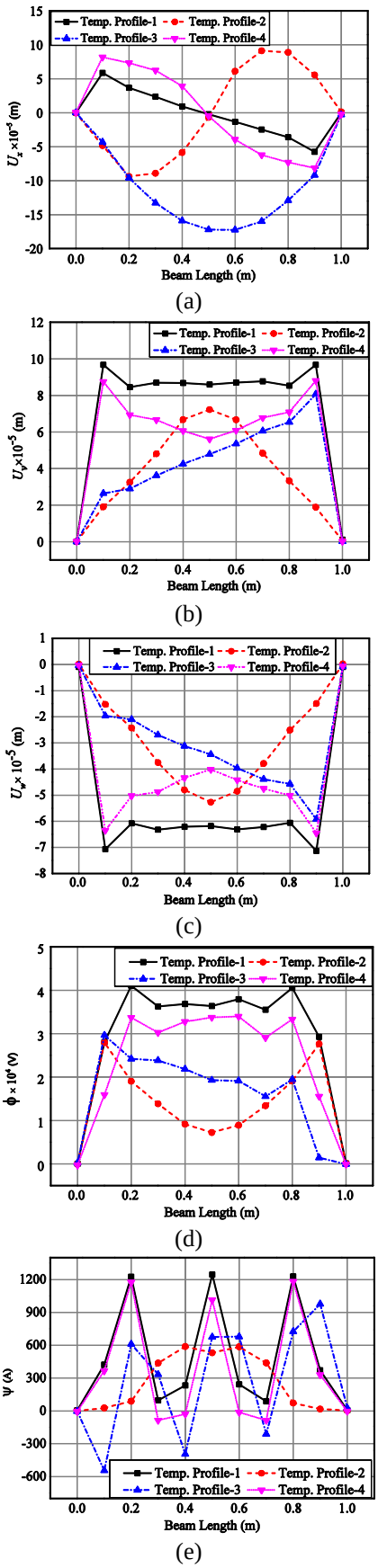


Fig. 8 Variation of (a) longitudinal $x$-direction ($U_x$) (b) $y$-direction ($U_v$) (c) $z$-direction ($U_w$) displacement components (d) electric potential ($\phi$) (e) magnetic potential ($\psi$) for various temperature profiles for C-C boundary condition

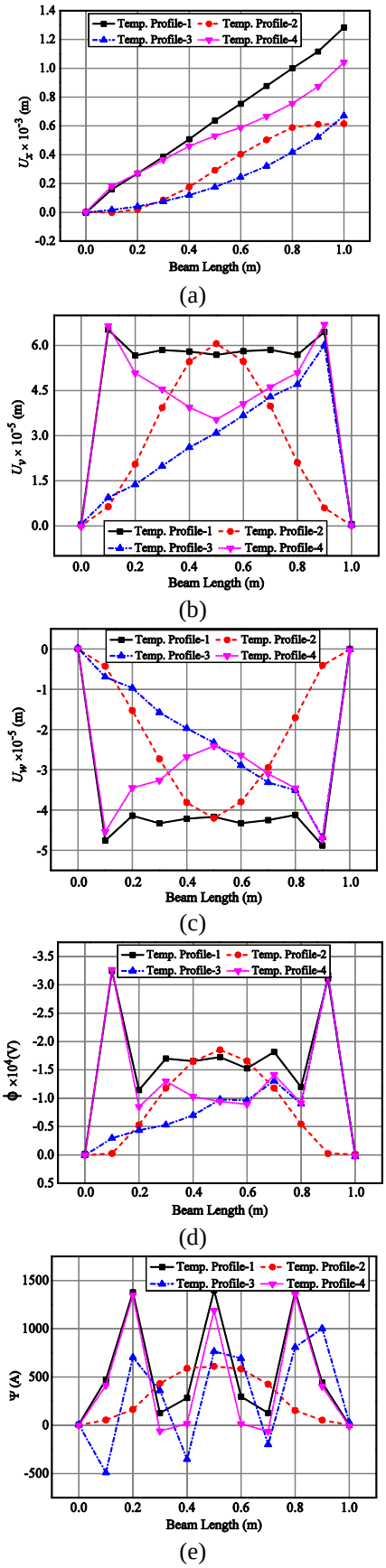


Fig. 9 Variation of (a) longitudinal *x*-direction ($U_x$) (b) *y*-direction ($U_v$) (c) *z*-direction displacement components ($U_w$) (d) electric potential ($\phi$) (e) magnetic potential ($\psi$) for various temperature profiles for C-S boundary condition

observed from Fig. 9(a) that the temperature profile-1 has more influence on the longitudinal *x*-direction displacement component $U_x$ while temperature profile-3 has the least effect. Further, $U_x$ varies along the length linearly from the clamped end to the free end of the MEE beam. From Figs. 9(b) and (c), it is evident that the *y*-direction displacement component $U_v$ and the transverse *z*-direction displacement component $U_w$ follows the same trend as shown in Figs. 8(b) and (c), respectively, for the clamped-clamped boundary condition. Figs. 9(d) and (e) illustrate the effect of temperature loading on the electrical potential and magnetic potentials, respectively. It may be observed from Fig. 9(d) that the variation of electric potential for temperature profile-1 and temperature profile-4 follows a similar trend. The unconstrained axial movement at the left support results in significant change of the electric potential as compared to the clamped-clamped (C-C) condition. While for the temperature profile-2, the variation of the electric potential in the clamped-simply supported beam is completely reversed than that of the clamped-clamped MEE beam (Fig. 8(d)). Further, it may be noticed from Fig. 9(e) that the variation of magnetic potentials for all the temperature profiles resembles the variation of the magnetic potential of the C-C MEE beam, but with a little higher magnitude. A smooth variation of magnetic potential is observed for temperature profile-2.

### *4.3 Parametric study*

The pyroelectric and pyromagnetic effects are observed in the system through the pyroelectric load and the pyromagnetic load, respectively. Thus, the developed pyroeffects are the outcome of cross coupling of thermo-electric and thermo-magnetic properties. These are generally termed as the cross properties or product properties of the system. These product properties influences the potentials directly, and displacements indirectly. Therefore, it is important to study the influence of boundary conditions on the product properties (pyroeffects). Also, the value of pyroelectric and pyromagnetic constants depends on the volume fraction of the system. Hence, the analysis of the MEE beam considering different volume fraction becomes prominent.

#### *4.3.1 Effect of product properties*

The clamped-clamped (C-C) and clamped-simply supported (C-S) MEE beams subjected to uniform temperature rise of 100 K is considered for the analysis. The material properties corresponding to the volume fraction $V_f$=0.5 are tabulated in Kondaiah *et al*. (2012). Influence of the product properties (pyroeffects) on the direct quantities (displacements and potentials) of the system is evaluated. Figs. 10-14 illustrate the comparison of the displacement components and the potentials for the C-C and C-F MEE beams with considering the pyro effects and conventional approach (without pyroeffects). It may be observed from these figures (Figs. 10-12) that the pyroeffects are negligible on the displacement components ($U_x$ ,$U_v$ ,$U_w$) of the MEE beam, while pyroeffects exhibit a significant variation in the electric potential for both the C-C and C-S beam as depicted in Fig. 13. It may be due to the

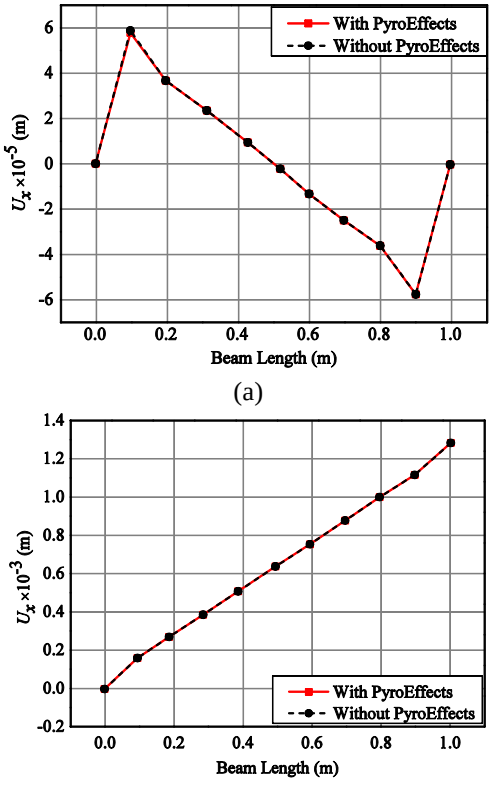


Fig. 10 Effect of product property on *x*-displacement component ($U_x$): (a) C-C boundary condition (b) C-S boundary condition

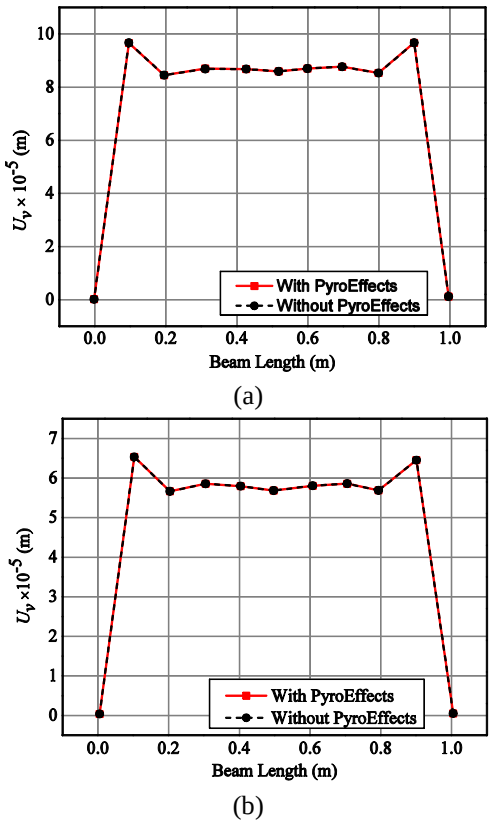


Fig. 11 Effect of product property on *y*-displacemen component ($U_v$): (a) C-C boundary condition (b) C-S boundary condition

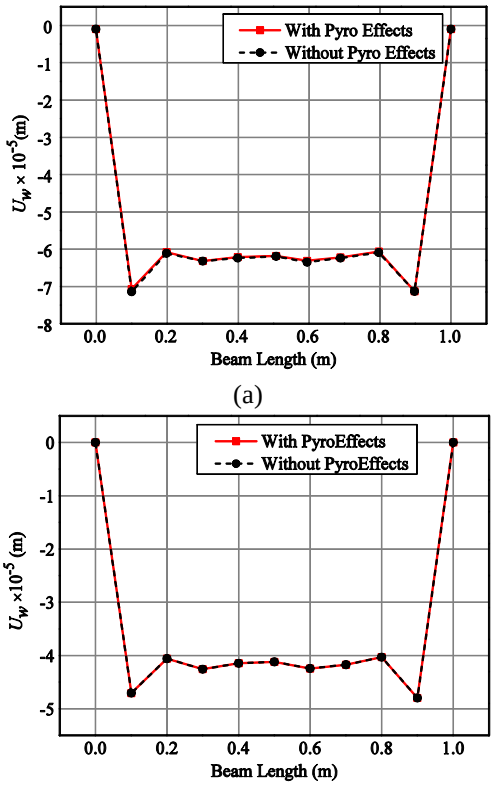


Fig. 12 Effect of product property on *z*-displacement component ($U_w$): (a) C-C boundary condition (b) C-S boundary condition

direct effect of the product properties on the electric potentials. For the C-S boundary condition, the pyroeffects tends to increase the electric potential of the MEE beam, whereas for the C-C MEE beam the pyroeffects reduces the electric potential. Fig. 14 depicts that the pyroeffects have a negligible influence on the magnetic potentials.

#### *4.3.2 Effect of volume fraction*

The effect of volume fraction of the $BaTiO_3$ and $CoFe_2O_4$ on the primary variables (displacements and potentials) of the MEE beam has been investigated by considering a uniform temperature rise of 100 K. The comparison between the primary variables of clamped-clamped (C-C) and clamped-simply supported (C-S) MEE beams are shown in Figs. 15-19. It may be observed from Figs. 15(a) and (b) that the effect of volume fraction on the *x*- direction displacement component is scanty for the C-C MEE beam while noticeable variations may be observed in case of C-S MEE beam. Also it may be noticed from Figs. 15(a) and 16(a) that the maximum longitudinal displacement ($U_x$) and y-direction displacement ($U_v$) occurs for the volume fraction $V_f$=0.0. However, for the C-S MEE beam, it is observed for the volume fraction $V_f$=1.0 as shown in Figs. 15(b) and 16(b). The maximum transverse *z*-direction displacement component for the C-C and C-S MEE beam is observed for $V_f$=0.2 and $V_f$=0.0, respectively. It may also be seen from Figs. 18(a) and (b) that for the volume fraction $V_f$=0.2, the electric potential is maximum for both the C-C and C-S MEE beams. Fig. 19(a) and (b)

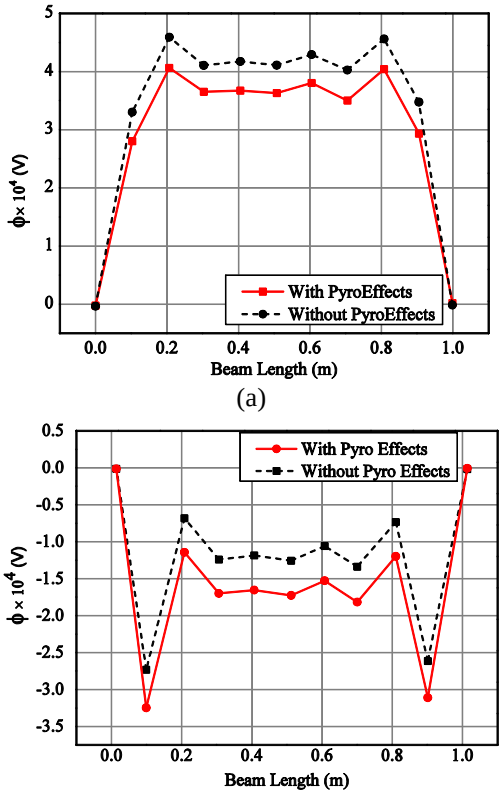


Fig. 13 Effect of product property on electric potential ($\phi$): (a) C-C boundary condition (b) C-S boundary condition

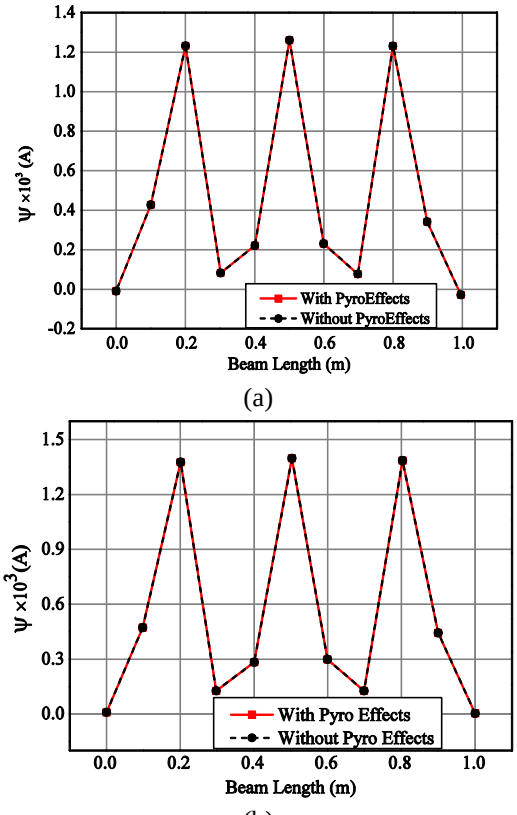


Fig. 14 Effect of product property on magnetic potential ($\psi$): (a) C-C boundary condition (b) C-S boundary condition

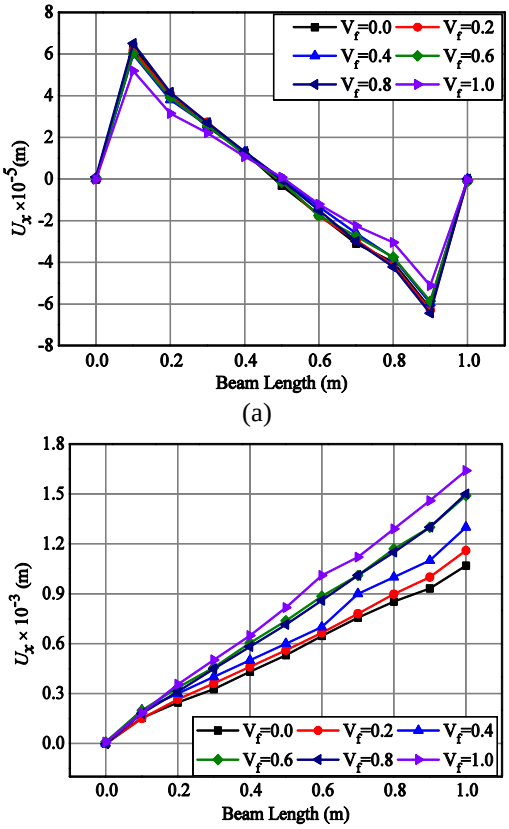


Fig. 15 Effect of volume fraction on *x*-displacemen component: (a) C-C boundary condition (b) C-S boundary condition

illustrate that the pure piezomagnetic material ($V_f$=0.0) exhibit the maximum magnitude of the magnetic potential while as expected for the volume fraction $V_f$=1.0, the magnetic potential is minimum for both the cases.

### *4.3.3 Effect of aspect ratio (L/h) on electric and magnetic potentials*

The effect of span length to thickness ratio ($L/h$) on the electric and magnetic potentials has been investigated by considering the clamped-free (C-F) and clamped-simply supported (C-S) MEE beam. Based on the $L/h$ ratio, the MEE beams are classified as deep ($0.5<L/h<2$), moderate ($2<L/h<6$) and shallow beams ($L/h>6$). In the present study, the thermal environment of uniform temperature rise $\Delta T$=100 K is assumed and the numerical values of $L/h$ considered for the analysis are 1.25, 3 and 10 for deep, moderate and shallow beams, respectively. Figs. 20(a) and (b) depict the characteristic behavior of the electric potential for the C-F and C-S beam, respectively. For both the boundary conditions, the deep MEE beam has a pronounced effect on the electric potential. Figs. 21(a) and (b) demonstrate the magnetic potential variation for the C-F and C-S MEE beams. It can be observed from these figures that for the C-F condition, moderate MEE beams ($L/h$=3) exhibit highest magnetic potential at the midspan of the beam whereas, for C-S condition, it is observed for the deep MEE beam.

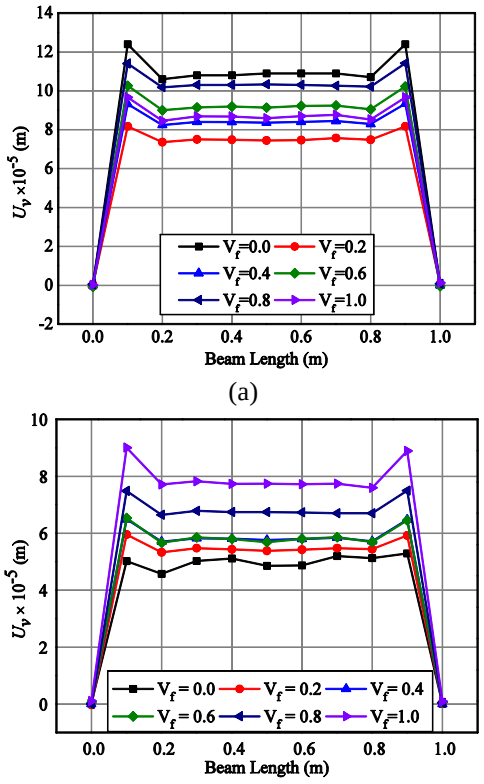


(a)




(b)

Fig. 16 Effect of volume fraction on *y*-displacement component: (a) C-C boundary condition (b) C-S boundary condition

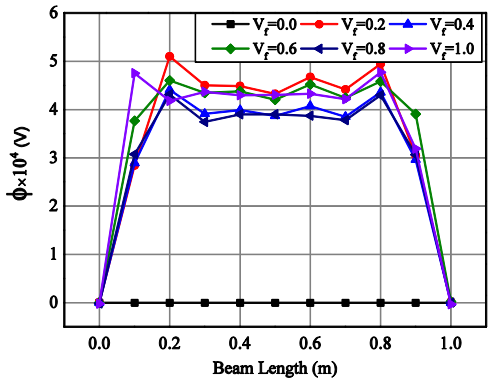


(a)

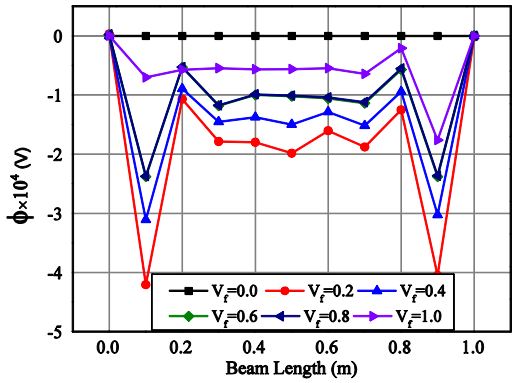


(b)

Fig. 18 Effect of volume fraction on electric potential ($\phi$) : (a) C-C boundary condition (b) C-S boundary condition

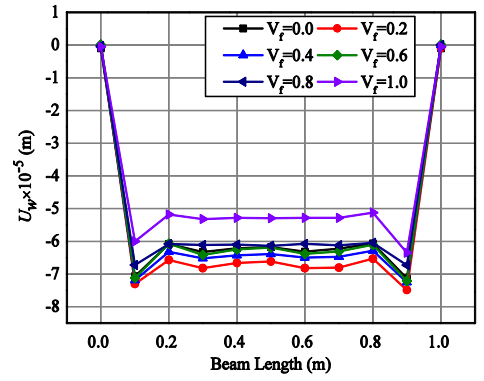


(a)

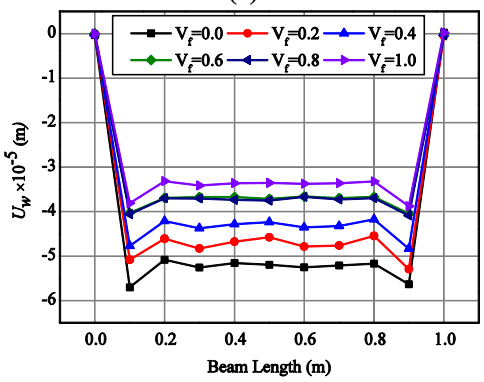


(b)

Fig. 17 Effect of volume fraction on *z*-displacement component: (a) C-C boundary condition (b) C-S boundary condition

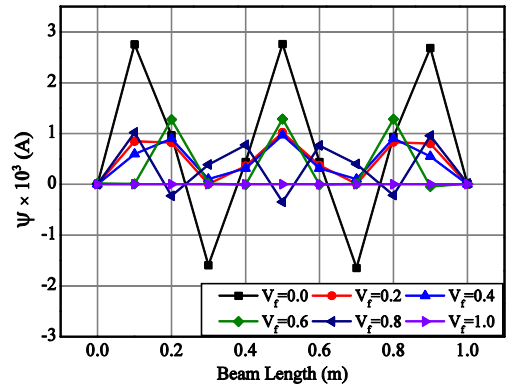


(a)

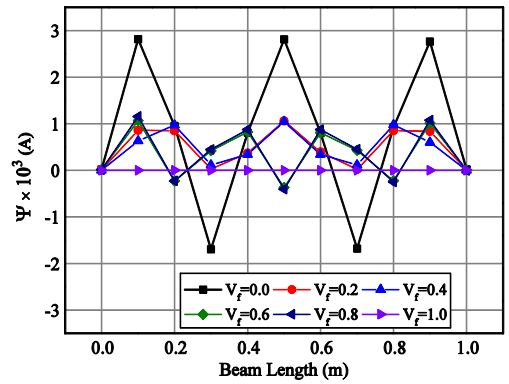


(b)

Fig. 19 Effect of volume fraction on magnetic potential ($\psi$): (a) C-C boundary condition (b) C-S boundary condition

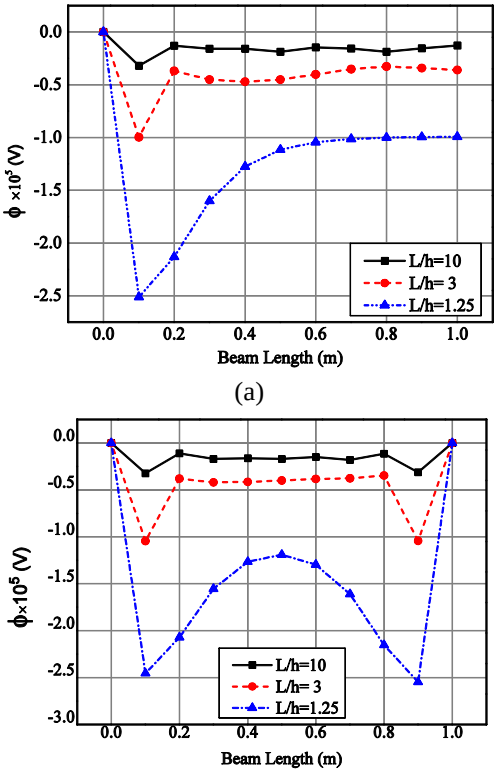


Fig. 20 Effect of aspect ratio on the electric potential: (a) C F (b) C-S boundary condition

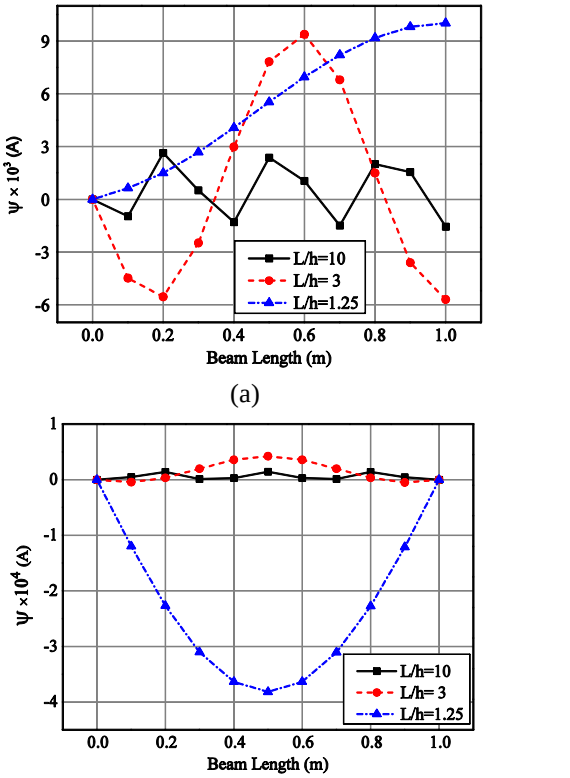


Fig. 21 Effect of aspect ratio on the magnetic potential: (a) C-F (b) C-S boundary condition

## 5. Conclusions

In this paper, the static behavior of a MEE beam subjected to various form of thermal loading and boundary conditions is studied using the finite element procedures. Influence of the pyroelectric and pyromagnetic effects on the direct quantities of the MEE beam is analyzed. Incorporating the Maxwell electrostatic and electromagnetic equations, variation of stresses, displacements, electric potential and magnetic potential along the length of the MEE beam has been investigated. The results obtained in present analysis reveal that, irrespective of the boundary conditions and the temperature profile, the pyroeffects exhibit negligible influence on the displacements and stresses of the MEE beam. It may due to negligible indirect effects of the pyroeffects. However, the pyroeffects show a dominant influence only on the electric potential developed in the system. For a clamped-free and clamped-simply supported MEE beam, the pyroeffects influence the increase of the electric potential while for the clamped-clamped MEE beam, a deteriorating effect may be observed. Among all the temperature profiles considered, the uniform temperature profile exhibit significant effect on the direct quantities. The maximum electric potential is observed for clamped-clamped boundary condition at the region near the clamped end of the MEE beam. Further, the comprehensive investigation on the influence of the volume fraction, aspect ratio and boundary conditions on the direct quantities of the MEE beam in the thermal environment suggests that for the volume fraction $V_f$=0.2, the maximum electric potential can be obtained. The moderate MEE beam (aspect ratio $L/h$=3) with clamped free boundary condition demonstrates the highest magnetic potential at the midspan of the beam, whereas for the clamped simply supported beam, it is observed for the aspect ratio $L/h$=1.25 (deep beam). It is expected that the results obtained in the present analysis can have a significant contribution in enhancing the design, performance and applicability of MEE smart structures in thermal environment.

## References

Annigeri, A.R., Ganesan, N. and Swarnamani, S. (2007), "Free vibration behavior of multiphase and layered magneto-electro-elastic beam", *J. Sound Vib.*, **299**, 44-63.

Ansari, R., Gholami, R. and Rouhi, H. (2015), "Size-dependent nonlinear forced vibration analysis of magneto-electro-thermo-elastic Timoshenko nanobeams based upon the nonlocal elasticity theory", *Compos. Struct.*, **126**, 216-226.

Badri, T.M. and Al-Kayiem, H.H. (2013), "Analytical solution for simply supported and multilayered Magneto-Electro-Elastic Plates", *Asian J. Sci. Res.*, **6**, 236-244

Beni, Y.T. (2016), "Size-dependent analysis of piezoelectric nanobeams including electro-mechanical coupling", *Mech. Res. Commun.*, **75**, 67-80.

Bhangale, R.K. and Ganesan, N. (2006), "Free vibration of simply supported functionally graded and layered magneto-electro-elastic plates by finite element method", *J. Sound Vib.*, **294**, 1016-1038.

Biju, B., Ganesan, N. and Shankar, K. (2011), "Dynamic response of multiphase magnetoelectroelastic sensors using 3D magnetic

vector potential approach", *IEEE Sens. J.*, **11**(9), 2169-2176.
Biju, B., Ganesan, N. and Shankar, K. (2012), "Effect of displacement current in magneto-electro-elastic plates subjected to dynamic loading", *Int. J. Mech. Mater. Des.*, **8**(4), 349-358.
Challagulla, K.S. and Georgiades, A.V. (2011), "Micromechanical analysis of magneto-electro-thermo-elastic composite materials with applications to multilayered structures", *Int. J. Eng. Sci.*, **49**, 85-104.
Chen, J., Chen, H., Pan, E. and Heyliger, P.R. (2007), "Modal analysis of magneto-electro-elastic plates using the state-vector approach", *J. Sound Vib.*, **304**, 722-734.
Chen, W.Q., Lee, K.Y. and Ding, H.J. (2005), "On free vibration of non homogeneous transversely isotropic magneto-electro-elastic plates", *J. Sound Vib.*, **279**, 237-251.
Daga, A., Ganesan, N. and Shankar, K. (2009), "Transient dynamic response of cantilever Magneto-Electro-Elastic beam using finite elements", *Int. J. Comput. Meth. Eng. Sci. Mech.*, **10**, 173-185
Ebrahimi, F. and Barati, M.R. (2016), "Dynamic modeling of a thermo-piezo-electrically actuated nanosize beam subjected to a magnetic field", *Appl. Phys. A*, **122**, 451.
Gornandt, A. and Gabbert, U. (2002), "Finite element analysis of thermopiezoelectric smart structures", *Acta Mechanica*, **154**, 129-140.
Gupta, V., Sharma, M., Thakur, N. and Singh, S.P. (2011), "Active vibration control of a smart plate using a piezoelectric sensor-actuator pair at elevated temperatures", *Smart Mater. Struct.*, **20,** 105023.
Hadjiloizi, D.A., Georgiades, A.V., Kalamkarov, A.L. and Jothi, S. (2013), "Micromechanical modeling of piezo-magneto-thermo-elastic composite structures: Part I Theory", *Eur. J. Mech. A/Solid.*, **39**, 298-312.
Hadjiloizi, D.A., Georgiades, A.V., Kalamkarov, A.L. and Jothi, S. (2013), "Micromechanical modeling of piezo-magneto-thermo-elastic composite structures: Part 2-Applications", *Eur. J. Mech. A/Solid.*, **39**, 313- 327.
Jandaghian, A.A. and Rahmani, O. (2016), "Free vibration analysis of magneto-electro thermo-elastic nanobeams resting on a Pasternak foundation", *Smart Mater. Struct.*, **25**, 035023.
Kattimani, S.C. and Ray, M.C. (2014), "Active control of large amplitude vibrations of smart magneto-electro-elastic doubly curved shells", *Int. J. Mech. Mater. Des.*, **10**(4), 351-378.
Kattimani, S.C. and Ray, M.C. (2014), "Smart damping of geometrically nonlinear vibrations of magneto-electro-elastic plates", *Compos. Struct.*, **14**, 51-63.
Kattimani, S.C. and Ray, M.C. (2015), "Control of geometrically nonlinear vibrations of functionally graded magneto-electro-elastic plates", *Int. J. Mech. Sci.*, **99**, 154-167.
Kim, J.Y., Li, Z. and Baltazar, A. (2012), "Pyroelectric and pyromagnetic coefficients of functionally graded multilayered multiferroic composites", *Acta Mechanica*, **223**, 849-860.
Kondaiah, P., Shankar, K. and Ganesan, N. (2012), "Studies on magneto-electro-elastic cantilever beam under thermal environment", *Coupl. Syst. Mech.*, **1**(2), 205-217
Kondaiah, P., Shankar, K. and Ganesan, N. (2013), "Pyroelectric and pyromagnetic effects on behavior of magneto-electro-elastic plate", *Coupl. Syst. Mech.*, **2**, 1-22.
Kumaravel, A., Ganesan, N. and Sethuraman, R. (2007), "Buckling and vibration analysis of layered and multiphase magneto-electro-elastic beam under thermal environment", *Multidisc. Model. Mater. Struct.*, **3**, 461-476.
Kumaravel, A., Ganesan, N. and Sethuraman, R. (2007), "Steady-state analysis of a three-layered electro-magneto-elastic strip in a thermal environment", *Smart Mater. Struct.*, **16**, 282-295.
Lage, R.G., Soares, C.M.M., Soares, C.A.M. and Reddy, J.N. (2004), "Layerwise partial mixed finite element analysis of magneto-electro-elastic plates", *Comput. Struct.*, **82**, 1293-1301.
Milazzo, A., Orlando, C. and Alaimo, A. (2009), "An analytical solution for the magneto-electro-elastic bimorph beam forced vibrations problem", *Smart Mater. Struct.*, **18**(8), 85012.
Ootao, Y. and Tanigawa, Y. (2005), "Transient analysis of multilayered magneto-electro-thermoelastic strip due to nonuniform heat supply", *Compos. Struct.*, **68**, 471-480.
Pan, E. (2001), "Exact solution for simply supported and multilayered Magneto-Electro-Elastic plates", *Tran. ASME*, **68**, 608-618.
Panda, S. and Ray, M.C. (2008), "Nonlinear finite element analysis of functionally graded plates integrated with patches of piezoelectric fiber reinforced composite", *Finite Elem. Anal. Des.*, **44,** 493-504.
Rahman, N. and Naushad Alam, M. (2015), "Structural control of piezoelectric laminated beams under thermal load", *J. Therm. Stress.*, **38**, 69-95.
Ramirez, F., Heyliger, P.R. and Pan, E. (2006), "Free vibration response of two-dimensional magneto-electro-elastic laminated plates", *J. Sound Vib.*, **292**, 626-644.
Ray, M.C. and Batra, R.C. (2008), "Smart constrained layer damping of functionally graded shells using vertically/obliquely reinforced 1-3 piezocomposite under a thermal Environment", *Smart Mater. Struct.*, **17**, 055007.
Ray, M.C., Bhattacharya, R. and Samanta, B. (1994), "Static analysis of an intelligent structure by the finite element method", *Comput. Struct.*, **52**, 617-631.
Sharnappa, G.N. and Sethuraman, R. (2010), "Thermally induced vibrations of piezo-thermo-viscoelastic-composite beam with relaxation times and system response", *Multidisc. Model. Mater. Struct.*, **6**(1), 120-140.
Sunar, M., Al-Garni, A.Z., Ali, M.H. and Kahraman, R. (2002), "Finite element modeling of thermopiezomagnetic smart structures", *AIAA J.*, **40**, 1845-1851.
Tauchert, T.R. (1996), "Cylindrical bending of hybrid laminates under thermo-electro-mechanical loading", *J. Therm. Stress.*, **19**, 287-296.
Vaezi, M., Shirbani, M.M. and Hajnayeb, A. (2016), "Free vibration analysis of magneto-electro-elastic microbeams subjected to magneto-electric loads", *Physica E*, **75**, 280-286.
Xin, L. and Hu, Z (2015), "Free vibration of layered magneto-electro-elastic beams by SS-DSC approach", *Compos. Struct.*, **125**, 96-103.

*CC*

## Appendix

The various stiffness matrices obtained during condensation method in the process of obtaining equivalent stiffness matrix and equivalent load vector are given below,

$$[K_1]=[K_{\phi t}]-[K_{\psi\phi}][K_{\psi\psi}]^{-1}[K_{\psi t}],$$

$$[K_2]=[K_{\phi\phi}]-[K_{\psi\phi}][K_{\psi\psi}]^{-1}[K_{\phi\psi}],$$

$$[K_3]=[K_2]^{-1}[K_1],$$

$$[K_4]=[K_2]^{-1}[K_{\psi\phi}][K_{\psi\psi}],$$

$$[K_5]=[K_{tt}]+[K_{t\psi}][K_{\psi\psi}]^{-1}[K_{\psi t}],$$

$$[K_6]=[K_{t\phi}]-[K_{t\psi}][K_{\psi\psi}]^{-1}[K_{\phi\psi}],$$

$$[K_7]=[K_5]+[K_6][K_3],\ [K_8]=[K_6][K_2]^{-1},$$

$$[K_9]=[K_{t\psi}][K_{\psi\psi}]^{-1}-[K_6][K_4],$$

$$[K_{eq}]=[K_7],$$

$$\{F_{eq}\}=[K_9]\{F_{pm}\}+[K_8]\{F_{pe}\}+\{F_{th}\}$$